nature portfolio

Peer Review File

Broadband near-infrared hyperbolic polaritons in MoOCl2

Corresponding Author: Dr Yaolong Li

This file contains all reviewer reports in order by version, followed by all author rebuttals in order by version.

Version 0:

Reviewer comments:

Reviewer #1

(Remarks to the Author)
In the present work Li et al. report on the measurement of hyperbolic plasmons at near-infrared frequencies through photoemission electron microscopy (PEEM). While hyperbolic modes have been extensively studied through sSNOM, the shift to plasmons and near-IR frequencies allowed their observation through PEEM, which has not been used before to image hyperbolic wavefronts. Additionally, the authors show that twisting two layers of MoOCl2 on top of each other can lead to canalized wavefronts, analogously to what has been shown at mid-IR frequencies in MoO3. They also show (again analogously to phonon polaritons) that circular patterns can be used to focus plasmons in MoOCl2 due to their hyperbolic propagation. Overall, this work contains an impressive amount of experimental data using for the first time PEEM to image the propagation of hyperbolic modes. However, the authors fail to cite relevant experimental work on MoOCl2. The theoretical description of hyperbolic modes also seems lacking. I think before considering for publication, the authors need to address the following concerns:

#1 – MoOCl2 plasmon polaritons have been recently demonstrated by sSNOM at visible and near-IR frequencies (10.1038/s41467-024-53988-7, 10.48550/arXiv.2406.05703). The authors ignore these works and give the impression in that they are reporting plasmon polaritons in MoOCl2 for the first time.

#2 – The theoretical analysis of the hyperbolic modes seems to be absent in the paper (only 3D electromagnetic simulations are shown). A detailed description of the IFCs of hyperbolic modes in thin layers has been developed for phonon polaritons (see for example 10.1103/PhysRevB.100.235408) and has recently been applied to MoOCl2 plasmons (10.1038/s41467-024-53988-7). In the present manuscript only a fit to the hyperbolic experimental IFCs is performed, with no comparison with the theoretical ones. The authors should perform such calculations and judge the agreement with their experiments. Similarly, the theory for polaritons in twisted bilayers has been developed but has not been applied in this work.

#3 – In Fig 2, below 700 nm one can clearly see 6 symmetric peaks in the FFT images, where do they come from? Why are they absent in the data above 900 nm? There also seem to be “hyperbolic” wavefronts along the y-direction in the FFT images at 600 and 550 nm, what are those?

#4 – The authors describe the oscillations observed below 700 nm to a “air mode”. However, previous works showed how “lenticular modes” can be excited in MoOCl2 under certain conditions (10.1038/s41467-024-53988-7), which share similar features with “leaky” phonon polaritons modes observed in calcite (10.1038/s41467-023-38326-7). The modes observed in the PEEM experiments are also clearly anisotropic, which suggests me these are not “air modes” as described in the text.

#5 – The authors use 200 nm Au nanoparticles with 5 nm SiO2 shells as plasmon polariton launchers Why do the particles have a 5 nm SiO2 shell? Does it play any role in the experiments?

#6 – I think the advantages of PEEM over sSNOM are not clear from the text. The use of normal incidence is cited as one advantage of PEEM. However, while often sSNOM is operated in reflection with tilted illumination, normal-incident transmission sSNOM has also been demonstrated (see for example 10.1021/nl101693a). No details are given about the time needed to perform one PEEM experiment, or how much the field of view can be changed, which could be advantages over sSNOM experiments.

#7 – In the first section of the SI it is mentioned that flakes are annealed at 120 degrees before measurement. Why is this procedure needed? What happens without annealing?

Reviewer #2

(Remarks to the Author)
The manuscript „Broadbacnd near-infrared hyperbolic polaritons in MoOCl2" by Li et al., contains a thorough non-linear photoelectron microscopy (PEEM) study of optically excited plasmon polaritons. The authors use the nowadays standard plasmonic imaging in PEEM and combine it with polarization-dependent excitation. Using Fourier techniques, the authors calculate iso-frequency contours that experimentally verify the hyperpolic shape of the plasmon's phase fronts.

The manuscript contains exciting data recorded on a rather new material. It is well written, very clear to read, and the experimental findings support the conclusions. I consider the manuscript clearly suitable for Nature Communications and I have only minor comments.

(1) The type of PEEM used is specified in the supplementary information, however, I think the manuscript would benefit from having that information in the main document. The reasoning for this is that there are many PEEMs around, with different capabilities and incidence geometries for the laser pulses. It is stated in line 64 of the main manuscript that the experiments were performed at "precisely normal incidence" (which is important for the interpretation of the data), and specifying the type of microscope used backs that claim.

(2) In some parts of the manuscript links to the supporting material focus on aspects that are not relevant to the manuscript and its story. In lines 163 to 168 of the main manuscript only references to the supplement are listed. Please consider, if the amount of material in the supplement is necessary. For instance, the Supplementary table S1 is nicely composed, but not necessary for the story. Furthermore, the Supplementary note around Figure S8 is in my opinion not relevant for the story either – in particular, as it provides no additional information that could not be obtained in Normal Incidence.

(3) When it comes to plasmons and imaging in Normal-Incidence PEEM, I believe the best reference would be Kahl et al., Plasmonics 9, 1401–1407 (2014). In this reference, normal-incidence PEEM was first applied to SPPs and the contrast differences between normal incidence PEEM and grazing incidence PEEM were discussed at large.

(4) Figure 2e has a scalebar missing. What are the white dots? Au particles?

(5) Figure 3 a-c are too small.

(6) In line 229 the authors claim plasmon focusing, but I did not find supporting data in Fig. 5 of the manuscript.

(7) Having attempted PEEM with MoOCl2 myself, I find the idea to perform the experiment at 85K to freeze the Cs on the substrate intriguing. As this is an important experimental detail, could the authors be more specific about the amount of Cs? How much was the work function changed? How did the authors conclude that it was only a sub-ML of CS?

(8) There are several minor grammar mistakes throughout the manuscript (mostly superfluous "the"), and the manuscript would benefit from a close read.

Reviewer #3

(Remarks to the Author)
The main finding reported in the manuscript is the observation of hyperbolic plasmon-polaritons (HPP) supported by two-dimensional crystals of MoOCl2 in the visible to the near-infrared range. Nevertheless, the previous publication "Visible-frequency hyperbolic plasmon polaritons in a natural van der Waals crystal", by Venturi, G., et al (Nat Commun 15, 9727, 2024), has recently shown and characterized the nanophotonics of HPP in MoOCl2. As a critical point, I could not find the citation of this reference in the manuscript. Moreover, the presented results do not add new aspects to the discussion provided in Venturi's work.
The use of PEEM to investigate the optical near field of bidimensional polaritonic media can be considered a novel technical approach, but the manuscript lacks presenting details on the technique and comparison to consolidated optical near field probes as s-SNOM. The work also lacks making quantitative comparison of the experimental results and data analysis with the simulations shown in the supplementary information. The results of polarization control and twisted crystals seem interesting but are only superficially discussed and no theoretical bases are provided to support and better describe the claimed control of the IFC and directionality. Therefore, I cannot recommend the publication. In the following, I list some points to be addressed to improve the work.
. Cite Venturi's work and point out the advances the manuscript presents.
. Improve the description of PEEM technique and provide details on how it can be used to probe the optical near field of polaritonic media. Provider for a comparison with s-SNOM.
. Improve data treatment. Extract polariton propagation profiles from the nanoparticles launchers, determine their momenta and construct the frequency-momentum dispersion relation that is a key property to understand the HPP's nanophotonics.
. Explain the changes in the central part of the FFTs in Fig. 2b.
. Verify why no HPP is seen for 700 nm excitation in Fig. 2 results. In Venturi's work HPPs are found around this wavelength.
. Justify the use of 5 nm SiO_2 @ 200 nm Au nanoparticles for polariton excitation, while larger metallic rod- or disk-like

antennae, without dielectric coatiangs, are typically designed for such functionalities.

Version 1:

Reviewer comments:

Reviewer #1

(Remarks to the Author)
The authors have addressed all my comment to the initial version of the manuscript, which I think is now suitable for publication in Nature Communications.

Reviewer #3

(Remarks to the Author)
The revised form of the manuscript has been considerably improved in comparison with the former one. The work now can be recommended for publication.

Point-to-point reply to the reviewers' comments.

We thank the reviewers for their careful reviewing of our manuscript and for their detailed and constructive reports. During the revision, we have taken all the comments from the reviewers into consideration. Our responses to each of the reviewers' comments are as follows and highlighted in blue, and the revisions in the new manuscript are highlighted in red.

Reviewer #1 (Remarks to the Author):

In the present work Li et al. report on the measurement of hyperbolic plasmons at near-infrared frequencies through photoemission electron microscopy (PEEM). While hyperbolic modes have been extensively studied through sSNOM, the shift to plasmons and near-IR frequencies allowed their observation through PEEM, which has not been used before to image hyperbolic wavefronts. Additionally, the authors show that twisting two layers of MoOCl2 on top of each other can lead to canalized wavefronts, analogously to what has been shown at mid-IR frequencies in MoO3. They also show (again analogously to phonon polaritons) that circular patterns can be used to focus plasmons in MoOCl2 due to their hyperbolic propagation. Overall, this work contains an impressive amount of experimental data using for the first time PEEM to image the propagation of hyperbolic modes. However, the authors fail to cite relevant experimental work on MoOCl2. The theoretical description of hyperbolic modes also seems lacking. I think before considering for publication, the authors need to address the following concerns:

Reply: We thank the referee for the helpful comments. We appreciate the referee' comment "this work contains an impressive amount of experimental data using for the first time PEEM to image the propagation of hyperbolic modes", which has captured the central idea of our work. We also thank the referee for the suggestions on citing relevant work on $MoOCl_2$ and adding theoretical description of hyperbolic modes, and we make the corresponding modifications.

Comment 1.1 MoOCl2 plasmon polaritons have been recently demonstrated by sSNOM at visible and near-IR frequencies (10.1038/s41467-024-53988-7, 10.48550/arXiv.2406.05703). The authors ignore these works and give the impression in that they are reporting plasmon polaritons in MoOCl2 for the first time.

Reply to 1.1: We thank the referee for pointing out this issue. Unfortunately, we were not aware of these two new publications.

Changes in the manuscript in answer to Comment 1.1: In the revised manuscript, we have cited the two relevant papers by s-SNOM published very recently, see [22,23]

Comment 1.2. The theoretical analysis of the hyperbolic modes seems to be absent in the paper (only 3D electromagnetic simulations are shown). A detailed description of the IFCs of hyperbolic modes in thin layers has been developed for phonon polaritons (see for example 10.1103/PhysRevB.100.235408) and has recently been applied to MoOCl2 plasmons (10.1038/s41467-024-53988-7). In the present manuscript only a fit to the hyperbolic experimental IFCs is performed, with no comparison with the theoretical ones. The authors should perform such calculations and judge the agreement with their experiments. Similarly, the theory for polaritons in twisted bilayers has been developed but has not been applied in this work.

Reply to 1.2: We thank the referee for the very helpful comments. We have added the theoretical analysis following the referee's suggestions in the revised Supporting Information, including the theoretical descriptions of IFCs, twisted bilayers, and comparisons with experimental results.

Changes in the manuscript in answer to Comment 1.2: The revised contents in the Supporting Information are as follow (see SI pages 5-6, 11-12):

Here, we present the theoretical descriptions of IFCs of hyperbolic modes supported by $MoOCl_2$ thin layers following the well-developed theory in the literature[19]. For the anisotropic medium $MoOCl_2$, the three principal components in dielectric permittivity tensor $\hat{\varepsilon}$ differ from each other.

$$\hat{\varepsilon} = \begin{pmatrix} \varepsilon_x & 0 & 0 \\ 0 & \varepsilon_y & 0 \\ 0 & 0 & \varepsilon_z \end{pmatrix} \tag{1}$$

We consider an $MoOCl_2$ thin slab between two isotropic media with dielectric permittivity ε_1 and ε_3, respectively. The dispersion relation for electromagnetic modes is given in Ref.[19]:

$$\left\{\alpha_x q_y^2 + \alpha_y q_x^2 + \frac{q_x^2+q_y^2}{2}\left(i\sqrt{q_x^2+q_y^2-\varepsilon_1} + i\sqrt{q_x^2+q_y^2-\varepsilon_3}\right)\right\}\left\{\alpha_x q_y^2 + \alpha_y q_x^2 + \frac{q_x^2+q_y^2}{2}\left(\frac{\varepsilon_1}{i\sqrt{q_x^2+q_y^2-\varepsilon_1}} + \frac{\varepsilon_3}{i\sqrt{q_x^2+q_y^2-\varepsilon_3}}\right)\right\} = q_x^2 q_y^2 (\alpha_x - \alpha_y)^2 \tag{2}$$

Where, $\alpha_{x,y} = \frac{k_0 d \varepsilon_{x,y}}{2i}$ are the normalized 2D effective conductivity components and d is thickness of the slab. In our case, $\varepsilon_1 = 1$ (air), $\varepsilon_3 = 1.5^2$ (glass) and $d = 40\ nm$.

In Fig. S6, the comparison of theoretical, simulated and experimental IFCs supported by a 40-nm $MoOCl_2$ flake at a representative wavelength of 1000 nm is presented. The calculated IFCs of hyperbolic mode are plotted as green dashed lines in Fig. S6c,d, which are in good agreement with the experimental and simulated FFT results. In Fig. S6c,d, the white and yellow cycles denote k_0 (air, n = 1) and $1.5k_0$ (substrate, n = 1.5), respectively, and appear to have some correspondence with the central region of the experimental FFT image, but the experimental signals are too low at the 1000 nm wavelength for the precise analysis. More detailed analysis will be presented later in the shorter wavelength region. In addition, the lenticular mode has little contribution at the 1000 nm wavelength, as shown by the small red dashed lines in Fig. S6c,d. It should be noted, in the simulation, the electric field monitor was 2 nm below the surface of $MoOCl_2$ to reduce the strong signals from the Au nanoparticle, and a logarithmic operation was performed on the electric field image before FFT to improve the signal quality.

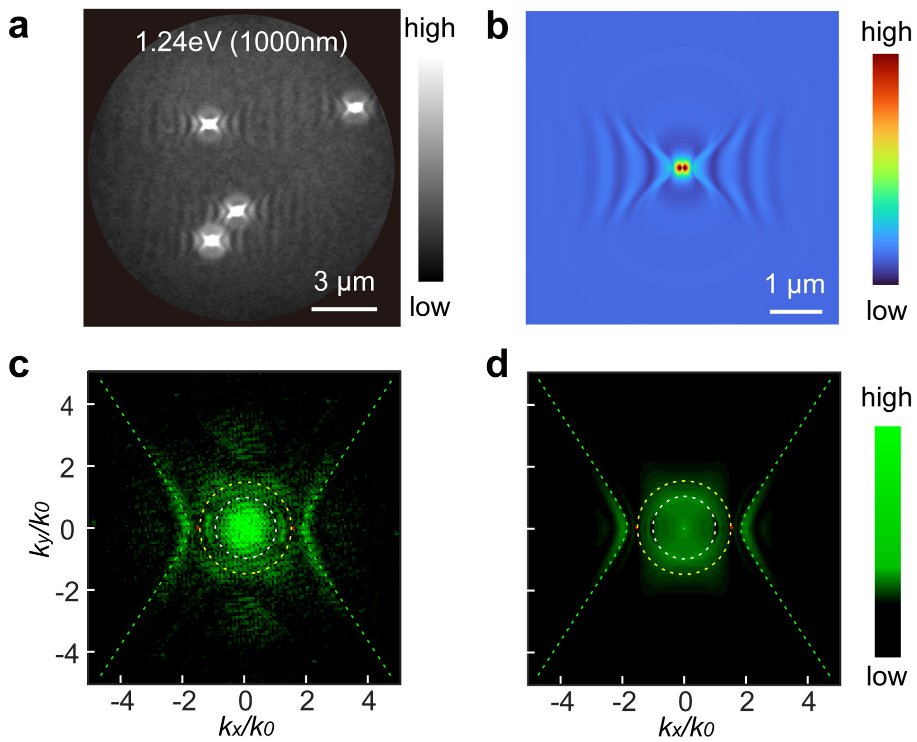

Fig. S6. Comparison of theoretical, simulated and experimental IFCs supported by a 40-nm $MoOCl_2$ flake (λ=1000 nm). **(a,c)** PEEM image from Fig. 2 and the corresponding IFCs. **(b,d)** Corresponding simulation results (electric field $|E|$ and FFT images). A logarithmic operation was performed on the electric field image before FFT to improve the signal quality. As illustrated in panels (c) and (d), the dashed lines represent theoretical results derived from Ref.[19]. The green dashed lines signify hyperbolic mode, while the white and yellow cycles denote k_0 (air, n = 1) and $1.5k_0$ (substrate, n = 1.5), respectively. The small red lines represent lenticular mode. The theoretical IFCs of hyperbolic mode are in good agreement with experimental and simulated results.

In addition, it can be seen that the asymptotes of the IFCs ($q_{x,y} \rightarrow \infty$) of hyperbolic modes in thin slab from Equation 2 coincide with the ones from the Fresnel equations:

$$\frac{q_y}{q_x} = \sqrt{-\frac{\alpha_x}{\alpha_y}} = \sqrt{-\frac{\varepsilon_x}{\varepsilon_y}} \tag{3}$$

This is why we use the hyperbolic equations to fit experimental data and calculate the open angle in Fig. 2f.

For the twisted bilayers, we assume a twist angle ($\Delta\theta$) between the top and the bottom flakes. The dielectric permittivity tensor of the top layer can be written as $R\begin{pmatrix}\varepsilon_x & 0\\ 0 & \varepsilon_y\end{pmatrix}R^T$, where $R=\begin{pmatrix}\cos\Delta\theta & -\sin\Delta\theta & 0\\ \sin\Delta\theta & \cos\Delta\theta & 0\\ 0 & 0 & 1\end{pmatrix}$ is the rotation matrix. The obtained dispersion from source-free Maxwell equations can be found in Ref.[22].

The IFCs in tBL $MoOCl_2$ flakes depend on the twist angle and the open angle of each layer in k space. We define the open angle as $\theta=\frac{\pi}{2}-\arctan\sqrt{-\varepsilon_x/\varepsilon_y}$ in Fig. 2b. The crossing of the IFCs in k space exhibits strong coupling between the top and bottom layers. And the number of anti-crossing points (N_{ACP}) determines the shape of the IFCs, i.e., hyperbolic or elliptic in tBL $MoOCl_2$ with different twist angles[22]. For the twist angle $\Delta\theta=2\theta$, the IFCs become flat and appear as two parallel asymptotic lines, so this angle is defined as topological transition angle. If $\Delta\theta<2\theta$, there are two anti-crossing points ($N_{ACP}=2$) and the corresponding hybridized IFCs are close to hyperbolic. Similarly, if $\Delta\theta>2\theta$, there are four anti-crossing points ($N_{ACP}=4$) and the hybridized IFCs are close to elliptic. In our experiments, at the representative wavelength of 1000 nm, the topological transition angle is $2\theta=62°$ for the thin $MoOCl_2$ flake, thus the images in Fig. 3 of the main text with twist angles of 52° and 90° present directional propagation and elliptical modes, respectively.

In addition, we have also added the theoretical calculations of dispersion relations and comparisons with experimental results. Specifically, we modified the old Fig. S7 and added corresponding descriptions. The revised contents in the Supporting Information are as follow (see SI pages 10-11):

We calculated the polariton dispersion relation by the transfer matrix method[21]. Our theoretical model is based on a three-layer structure: layer 1 ($z>0$, air), layer 2 ($-d<z<0$, $MoOCl_2$) and layer 3 ($z<-d$, glass), where z is the value of the vertical axis and d is the thickness of $MoOCl_2$ slab. We consider transverse magnetic modes and the corresponding Fresnel reflection coefficient r_p of this three-layer system is given by:

$$r_p=\frac{r_{12}+r_{23}e^{i2k_z^{(2)}d}}{1+r_{12}r_{23}e^{i2k_z^{(2)}d}} \tag{4}$$

$$r_{12}=\frac{Q_1-Q_2}{Q_1+Q_2} \tag{5}$$

$$r_{23}=\frac{Q_2-Q_3}{Q_2+Q_3} \tag{6}$$

$$Q_j=\frac{k_z^{(j)}}{\varepsilon_t^{(j)}} \tag{7}$$

$$k_z^{(j)} = \sqrt{\varepsilon_t^{(j)} \frac{\omega^2}{c^2} - \frac{\varepsilon_t^{(j)}}{\varepsilon_z^{(j)}} q^2} \quad (8)$$

$$\varepsilon_t^{(j)} = \varepsilon_x^{(j)} \cos^2\theta + \varepsilon_y^{(j)} \sin^2\theta \quad (9)$$

Here, $k_z^{(j)}$ is the out-of-plane wave vector, q is the in-plane wave vector, $\varepsilon_t^{(j)}$ is the tangential component of the in-plane dielectric function of layer j and θ is the angle relative to the x-axis. r_{jk} represents the reflection coefficient of the interface between layer j and layer k. When $Im(r_p)$ reach peaks, the dispersion relation can be derived. It should be noted, the permittivity of $MoOCl_2$ used here is from our measurements. As shown in Fig S8c, the calculated and experimental dispersion relations are in good agreement. In addition, the calculated wavevector-thickness relation is also consistent with the experimental result (Fig S8f). These results indicate that our entire work is self-consistent.

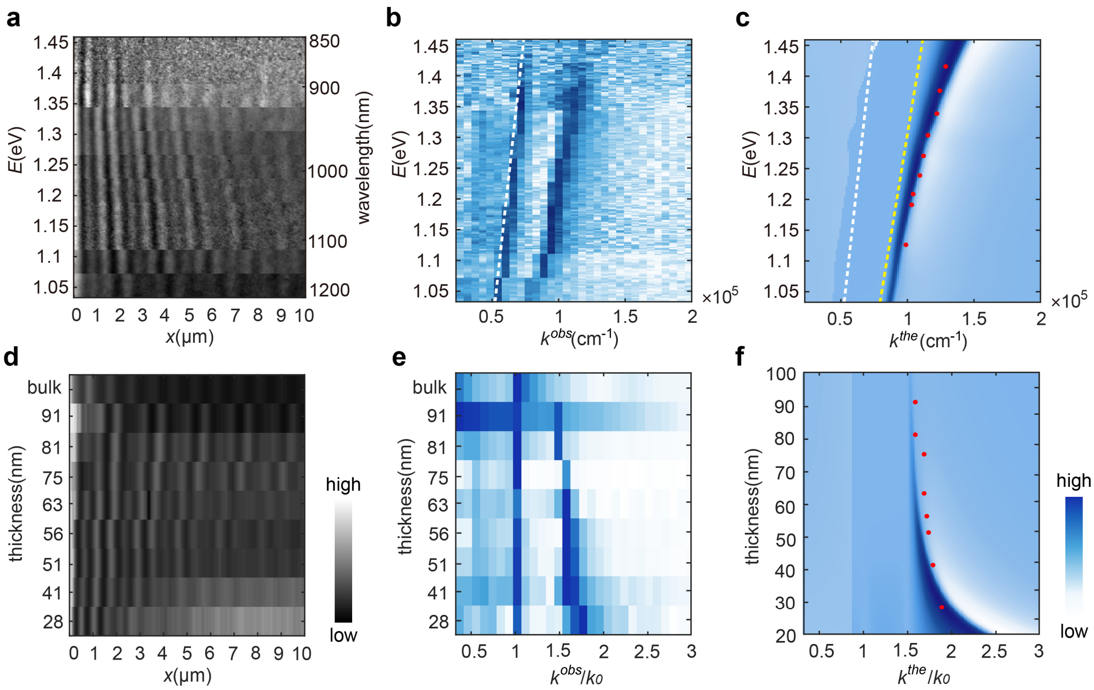

Fig. S8. Dispersion relation measured from $MoOCl_2$ sample edges and comparisons with theoretical calculations. (**a**) Wavelength-dependent near-field patterns on a straight sample edge (along the y-axis) of a ~60 nm $MoOCl_2$ flake excited with x-polarizations at normal incidence. (**b**) Extracted dispersion relation using FFT, in which the air mode and hyperbolic plasmon polariton mode can be observed. (**c**) Calculated polariton dispersion relation by transfer matrix method[21]. The red dots denote experimental results from (b). The white and yellow dashed lines denote air (k_0) and substrate ($1.5k_0$) modes. (**d,e**) Variations of near-field patterns and the corresponding FFT peaks with the thickness of $MoOCl_2$ (including bulk material), at a representative wavelength of 1000 nm. (**f**) Calculated polariton wavevector-thickness relation. The red dots denote experimental results from (e).

Comment 1.3. In Fig 2, below 700 nm one can clearly see 6 symmetric peaks in the

FFT images, where do they come from? Why are they absent in the data above 900 nm? There also seem to be "hyperbolic" wavefronts along the y-direction in the FFT images at 600 and 550 nm, what are those?

Reply to 1.3: Below 700 nm, the symmetric peaks and "hyperbolic wavefronts along the y-direction" in the FFT images are artifacts caused by the strong signals from Au nanoparticles during FFT operation. At these short wavelengths (below 700 nm), the signal intensities from Au nanoparticles are much stronger than that from $MoOCl_2$ surface, in order to reduce the signals from Au during FFT, we set a threshold for the maximum intensity of Au nanoparticles, but this causes additional artifacts, as founded by you. Specifically, if the threshold is set too high, the symmetric peaks will appear; if the threshold is set too low, the "hyperbolic wavefronts along the y-direction" will appear.

Changes in the manuscript in answer to Comment 1.3: To eliminate these artifacts, we have chosen a more appropriate threshold, and indeed much better results are presented in the revised Figure 2 of the main text. In the revised Figure 2, we have also plotted the air-mode cycles in the FFT images below 700 nm, which appear to overlap well with the experimental results in general.

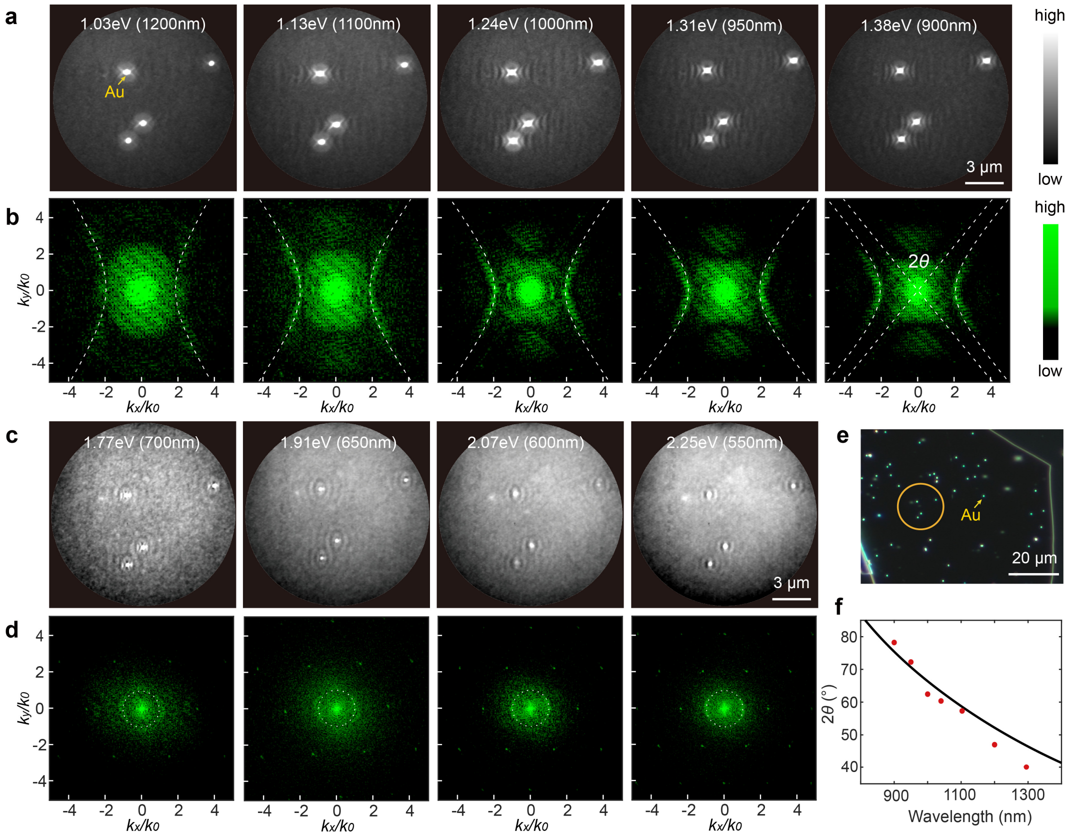

Revised Figure 2 of the main text

Comment 1.4. The authors describe the oscillations observed below 700 nm to a "air mode". However, previous works showed how "lenticular modes" can be excited in

MoOCl2 under certain conditions (10.1038/s41467-024-53988-7), which share similar features with “leaky” phonon polaritons modes observed in calcite (10.1038/s41467-023-38326-7). The modes observed in the PEEM experiments are also clearly anisotropic, which suggests me these are not “air modes” as described in the text.

Reply to 1.4: We have carefully considered this point, taking into account the highly valuable suggestions made by the referee. According to the theory in References (10.1103/PhysRevB.100.235408, 10.1038/s41467-023-38326-7), we calculated the IFCs of hyperbolic and lenticular modes in our sample at short wavelengths (below 700 nm), and the results are shown in Fig. R1c as green and red dashed lines, respectively. We also plotted the cycles of k_0 (air, n = 1) and $1.5k_0$ (substrate, n = 1.5) for comparison. As we can see in Fig. R1c, under x-polarization, the hyperbolic and lenticular modes in experimental IFCs cannot be clearly observed, possibly due to the high loss and low excitation efficiency of these modes in real samples at these short wavelengths. However, we can still observe 1−2 fringes of hyperbolic-like modes at 650−700 nm in real-space PEEM images. That is, although these modes exist in theory, they are too weak to be clearly observed in our experimental IFCs. On the other hand, in Fig. R1c, the experimental data generally overlaps with the air-mode cycle, thus we conclude that the observed modes are dominated by the air modes at short wavelengths under x-polarization, especially below 650 nm.
To better understanding this issue, we also checked the PEEM images under y-polarization excitation at these short wavelengths. As shown in Fig. R1d-f, two modes can be clearly observed in 700−550 nm, which generally overlap with the cycles of k_0 and $1.5k_0$. The k_0 mode is definitely air mode. For the mode close to $1.5k_0$, one might attribute it to air mode at the substrate interface at the first glance. However, it’s in fact TE_0 waveguide modes propagating along the X-direction under y-polarization, with an effective refractive index close to 1.5, due to the very thin thickness of the $MoOCl_2$ flake here (see mode analysis in Fig. R2). For a close look, along the k_x-direction, we see that the k value is always slightly larger than $1.5k_0$ and the deviation from $1.5k_0$ becomes larger when the wavelength decreases from 700 nm to 550 nm, which is consistent with the prediction of waveguide mode. We also noticed that such a waveguide mode is anisotropic due to strong anisotropy of $MoOCl_2$, as can be seen in both the PEEM images and the IFCs.
Upon further careful check and evaluation of the waveguide mode under y-polarization, we conclude that it is in fact the so-called lenticular mode, which is in perfect agreement with the prediction of theoretical calculations (Fig. R1f). Our result indicates that the lenticular mode in thin $MoOCl_2$ slab is closer to TE mode propagating along the X-direction and is thus polarization-dependent. The lenticular mode can be effectively excited with y-polarization, while the excitation efficiency with x-polarization is much lower, which is why we didn’t observe the lenticular mode with x-polarization, as demonstrated above. The experimental and theoretical results under y-polarization can also be well reproduced by simulations, as shown in Fig. R3. We have also checked how the lenticular modes change with the refractive index of the substrate in both

theoretical calculations and simulations, and they are perfectly consistent (not shown here).

Furthermore, we have found that the excitation efficiency of air mode is actually also polarization dependent, the intensity of air mode excited with TM polarization is considerably stronger than that with TE, that is why usually only half of the k_0 cycle can be observed under a given polarization. It should be noted that the polarization-dependent excitation efficiency of the air mode is not due to material anisotropy but rather is an inherent property of the air mode. More discussions on air mode can be found in literature, where it's also called quasicylindrical wave (Advanced Photonics Research 3, 2100354 (2022)). We would also like to point out a "strange problem" at short wavelengths under x-polarization, especially at 650 nm in Fig. R1a. That is, the wavefront looks very elliptical, but the modes along the x and y axes are both attributed to the air mode. The elliptical wavefront is caused by the initial phase delay near the point source for TE and TM modes, resulting in elliptical fringes by interference with the incident light. To make this argument more convincing, we have simulated the case of air modes at the surface of bulk SiO_2 excited from an Au nanoparticle. As shown in Fig. R4, "clearly anisotropic" elliptical fringes can be observed.

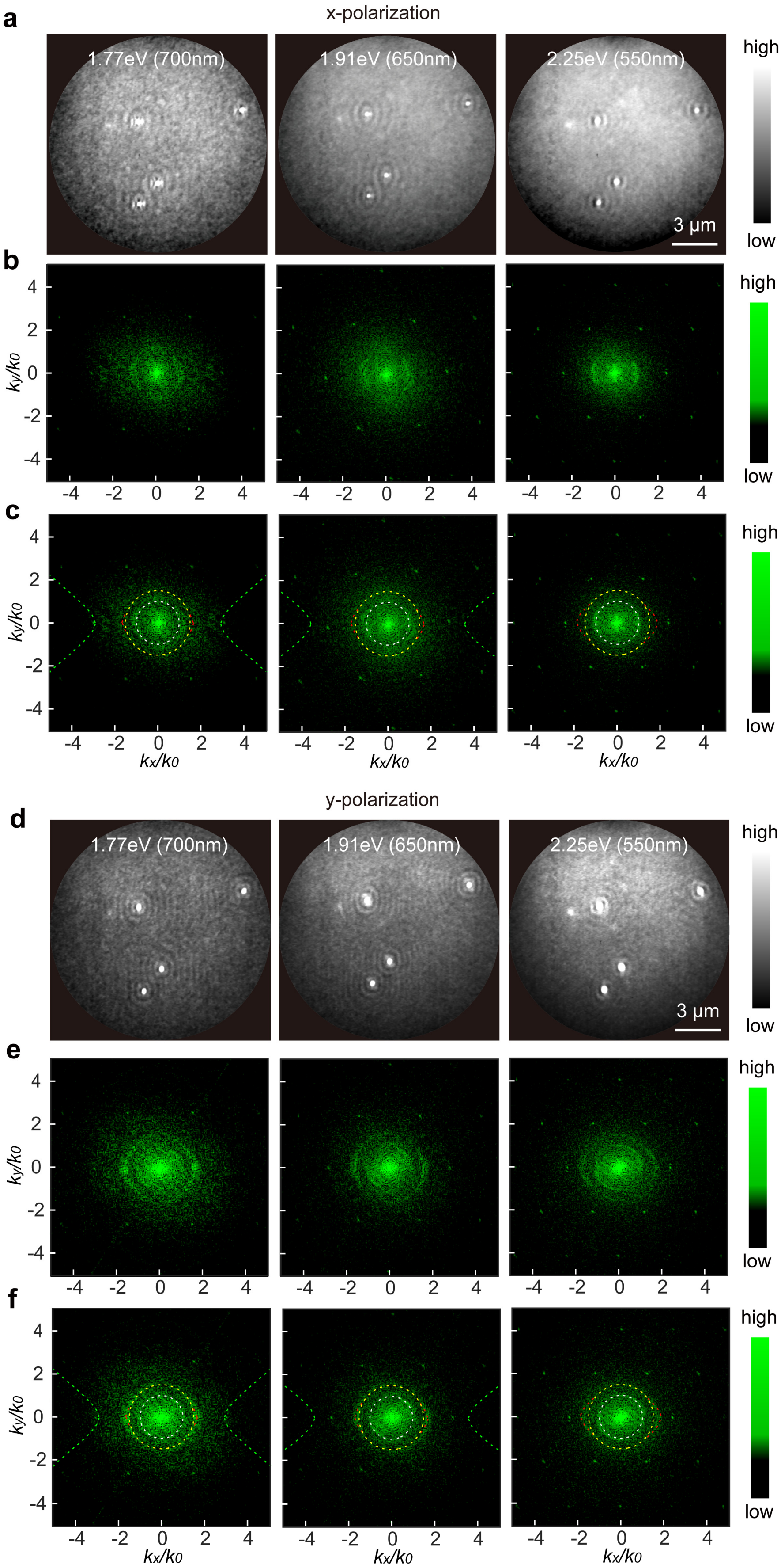
a
x-polarization
1.77eV (700nm)
1.91eV (650nm)
2.25eV (550nm)
3 μm
high
low
b
c
k_y/k_0
k_x/k_0
d
y-polarization
e
f

Fig. R1. PEEM and IFCs images at short wavelengths with x- (**a,b**) and y- (**d,e**) polarizations, respectively. Comparisons of experimental and theoretical IFCs are shown in panels (**c**) and (**f**), where the dashed lines represent theoretical calculations. The green lines signify hyperbolic mode, the red lines represent lenticular mode. The white and yellow cycles denote k_0 (air, n = 1) and $1.5k_0$ (substrate, n = 1.5), respectively.

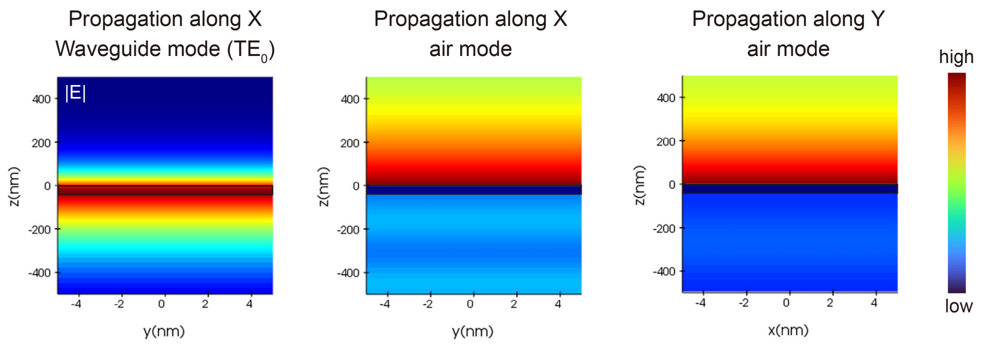

Fig. R2. Mode analysis of air/40 nm $MoOCl_2$/glass structure at a wavelength of 650 nm, propagating along X and Y-directions. For propagation along the X-direction, waveguide mode (TE_0, can be excited with y-polarization) and air mode (TM is stronger than TE) can be supported, while only air mode (TM is stronger than TE) can be propagated along Y-direction.

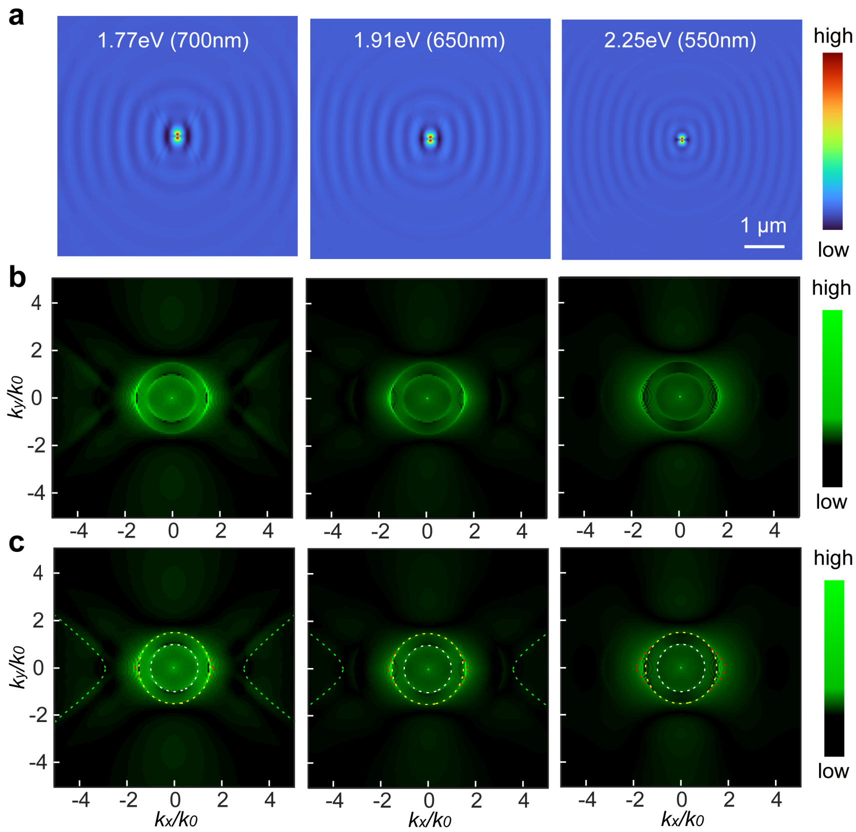

Fig. R3. Simulation results (mode profile |E| and FFT images) with y-polarization, showing clear lenticular modes in good agreement with theoretical calculations.

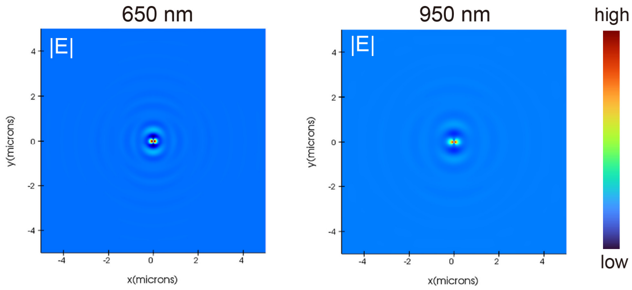

Fig. R4. Air modes at the surface of bulk SiO_2 excited from a 200 nm Au nanoparticle, with normal incidence at x-polarization (with the same simulation condition for Au nanoparticle on $MoOCl_2$).

Changes in the manuscript in answer to Comment 1.4: To address the referee's suggestion, we have added the extensive discussions above and Figure R1 in the Supporting Information (see pages 6-10).
We have also added some discussions in the main text (see page 6): See Figs. S5-S7 and further discussion on mode analysis in the Supporting Information, including hyperbolic and air modes, as well as the lenticular mode, the latter of which can be significantly excited at short wavelengths with y-polarization.

Comment 1.5. The authors use 200 nm Au nanoparticles with 5 nm SiO2 shells as plasmon polariton launchers Why do the particles have a 5 nm SiO2 shell? Does it play any role in the experiments?

Reply to 1.5: The referee is right, the 5nm SiO_2 shell is a useful trick for successful PEEM experiments. The main problem is the material-dependent intensity of the photoemission effect. The photoemission signals from bare Au nanoparticles are very strong due to the high free electron density of Au and the localized surface plasmon resonance (LSPR). Such strong photoemission will mask the signals from the $MoOCl_2$ surface, which has much weaker photoemission intensity.
To reduce the photoemission intensity of Au nanoparticles, we coated them with 5 nm SiO_2 shells because the free-electron density of SiO_2 is much lower than that of Au.

Changes in the manuscript in answer to Comment 1.5: We have added some descriptions of the role of the 5 nm SiO_2 shell in the Methods section of the revised main text, as follow (see page 10): The 5 nm SiO_2 shell was used to reduce the photoemission intensity of bare Au nanoparticle, which is an essential trick for successful PEEM experiments.
We also added a detailed discussions about the advantage of the SiO_2 shell in the Supporting Information (see SI page 20): The 5 nm SiO_2 shell is a very useful trick for successful PEEM experiments. The main problem is the material-dependent intensity of the photoemission effect. The photoemission signals from bare Au nanoparticles are very strong due to the high free electron density of Au and the localized surface plasmon

resonance (LSPR). Such strong photoemission will mask the signals from the $MoOCl_2$ surface, which has much weaker photoemission intensity.
To reduce the photoemission intensity of Au nanoparticles, we coated them with 5 nm SiO_2 shells because the free-electron density of SiO_2 is much lower than that of Au.

Comment 1.6. I think the advantages of PEEM over sSNOM are not clear from the text. The use of normal incidence is cited as one advantage of PEEM. However, while often sSNOM is operated in reflection with tilted illumination, normal-incident transmission sSNOM has also been demonstrated (see for example 10.1021/nl101693a). No details are given about the time needed to perform one PEEM experiment, or how much the field of view can be changed, which could be advantages over sSNOM experiments.

Reply to 1.6: First, we would like to emphasize that we prefer to avoid any statement that PEEM is superior to sSNOM. Science is not advanced by pitting different complementary techniques against each other. We agree with the referee that the transmission s-SNOM from the backside of transparent substrate and sample is also capable of normal incidence. Again, PEEM and sSNOM are complementary methods for studying hyperbolic plasmons at near-infrared frequencies, each with its own advantages. As mentioned by the referee, PEEM has the advantage of direct imaging. This leads to a faster detection scheme. The acquisition time of each image is typically 0.1-1.0 s, and multiple time averaging is often used only to further increase the signal-to-noise ratio. In addition, the field of view can be quickly switched (within a few seconds) from 100 μm to 0.75 μm with our PEEM type (ACSPELEEM III, Elmitec GmbH).

Changes in the manuscript in answer to Comment 1.6: To address the referee's comment, we have added some discussions in the Supporting Information (see page 19: Due to the non-scanning detection scheme, PEEM has the advantage of direct imaging. This leads to a faster detection scheme. The acquisition time of each image is typically 0.1-1.0 s, and multiple time averaging is often used only to further increase the signal-to-noise ratio. In addition, the field of view can be quickly switched (within a few seconds) from 100 μm to 0.75 μm with our PEEM type (ACSPELEEM III, Elmitec GmbH).

Furthermore, the non-scanning nature of PEEM results in very low near-field perturbation of the structured sample with high spatial resolution. PEEM is perfectly compatible with tunable femtosecond lasers in normal or oblique incidence, allowing convenient wavelength and polarization control and even time-resolved measurements on the fs time scale. For s-SNOM, oblique incidence from the front side is commonly used, but normal incidence has also been performed by transmission s-SNOM from the back side of the substrate[27].

Comment 1.7. In the first section of the SI it is mentioned that flakes are annealed at 120 degrees before measurement. Why is this procedure needed? What happens without annealing?

Reply to 1.7: UHV annealing is a common process for loading a sample from the air into a PEEM chamber. The main function is to remove water vapor and other adsorbates from the surface of the sample.

Changes in the manuscript in answer to Comment 1.7: To address the referee's comment, we have added some descriptions in the Supporting Information (see SI page 20): UHV annealing is a common process for loading a sample from the air into a PEEM chamber. The main function is to remove water vapor and other adsorbates from the surface of the sample.

Reviewer #2 (Remarks to the Author):
The manuscript, Broadband near-infrared hyperbolic polaritons in $MoOCl_2$" by Li et al., contains a thorough non-linear photoelectron microscopy (PEEM) study of optically excited plasmon polaritons. The authors use the nowadays standard plasmonic imaging in PEEM and combine it with polarization-dependent excitation. Using Fourier techniques, the authors calculate iso-frequency contours that experimentally verify the hyperpolic shape of the plasmon's phase fronts.
The manuscript contains exciting data recorded on a rather new material. It is well written, very clear to read, and the experimental findings support the conclusions. I consider the manuscript clearly suitable for Nature Communications and I have only minor comments.

Reply:
We thank the referee for the very positive comments. We have considered all of the following comments into our revision.

Comment 2.1. The type of PEEM used is specified in the supplementary information, however, I think the manuscript would benefit from having that information in the main document. The reasoning for this is that there are many PEEMs around, with different capabilities and incidence geometries for the laser pulses. It is stated in line 64 of the main manuscript that the experiments were performed at "precisely normal incidence" (which is important for the interpretation of the data), and specifying the type of microscope used backs that claim.

Reply to 2.1: We thank the referee for this valuable suggestion**.**

Changes in the manuscript in answer to Comment 2.1: We have adopted this suggestion, and added the Methods section to the main text, see page 12.

Comment 2.2. In some parts of the manuscript links to the supporting material focus on aspects that are not relevant to the manuscript and its story. In lines 163 to 168 of the main manuscript only references to the supplement are listed. Please consider, if the amount of material in the supplement is necessary. For instance, the Supplementary table S1 is nicely composed, but not necessary for the story. Furthermore, the Supplementary note around Figure S8 is in my opinion not relevant for the story either – in particular, as it provides no additional information that could not be obtained in Normal Incidence.

Reply to 2.2: We can agree with the referee that Figure S8 (excitation with oblique incidence) is not necessary for the main story.

Changes in the manuscript in answer to Comment 2.1: We have deleted Figure S8 in the revised manuscript. In addition, the sentence "Furthermore, oblique incidence excitations were performed in the PEEM experiments (Fig. S8)" is deleted in the manuscript (see page 6). In the Supporting Information, the entire section "Excitation with oblique incidence" is also deleted (see page 14). Regarding Table S1, we still think that this table is useful for readers who are not familiar with this field to learn about the properties of $MoOCl_2$ compared to other polariton materials. Therefore, we prefer to keep this section.

Comment 2.3. When it comes to plasmons and imaging in Normal-Incidence PEEM, I believe the best reference would be Kahl et al., Plasmonics 9, 1401–1407 (2014). In this reference, normal-incidence PEEM was first applied to SPPs and the contrast differences between normal incidence PEEM and grazing incidence PEEM were discussed at large.

Reply to 2.3: We have cited this reference in our revised manuscript as Ref. [24], and cited it at the position where normal-incidence PEEM is first mentioned (page 2).

Comment 2.4. Figure 2e has a scalebar missing. What are the white dots? Au particles?

Reply to 2.4: We have added the scalebar in Figure 2e in the revised version. Figure 2e is a dark-field image of our sample under a light microscope with a color camera. The white dots are indeed dark-field scattering of Au particles. To make this clear, we have added an "Au" label in Figure 2e.

Comment 2.5. Figure 3 a-c are too small.

Reply to 2.5: We have enlarged Figure 3 a-c in the revised version.

Comment 2.6. In line 229 the authors claim plasmon focusing, but I did not find supporting data in Fig. 5 of the manuscript.

Reply to 2.6: Unlike the Au SPP, the focusing for the $MoOCl_2$ hyperbolic plasmon occurs outside the ring slit. As can be seen in Figure 5b and 5e and also in Figure 5c, the focusing is observed outside the ring slit. It should be noted that such focusing is not as strong as in Au SPP due to the short propagation length of the MoOCl2-assisted hyperbolic plasmon, which may be the reason for the difficulty in finding the focusing.

Comment 2.7. Having attempted PEEM with MoOCl2 myself, I find the idea to perform the experiment at 85K to freeze the Cs on the substrate intriguing. As this is an important experimental detail, could the authors be more specific about the amount of Cs? How much was the work function changed? How did the authors conclude that it was only a sub-ML of Cs?

Reply to 2.7: The use of low temperature for Cs adsorption on the surface of $MoOCl_2$ is indeed essential for our PEEM experiments. It's well known that it's rather easy to deposit Cs on Au film, ITO and other substrates, even at room temperature. However, we find that it's much more challenging to deposit Cs atoms on a $MoOCl_2$ surface. Therefore, we moved to low temperature and reduced the kinetic energy of Cs movement on the surface of $MoOCl_2$, a strategy that worked quite well.
Cs deposition was performed with an alkali metal dispenser (SAES), and the amount of Cs was controlled by the evaporation current and time. In our experiments, the current was set to 5.7 A, and the time is less than 40 s. The work function was estimated to be slightly less than 2.5 eV after Cs deposition, since the photoemission at 1000 nm wavelength is still a two-photon mechanism (SI, Fig. S3). It is well known that less than 0.1ML Cs is required for such a strong reduction of the work function, see e.g., Journal of the Franklin Institute Volume 298, Issue 4, October 1974, pages 255-256.

Changes in the manuscript in answer to Comment 2.7: We have added some discussion on Cs deposition in the Supporting Information, as follow (see SI page 20): Cs deposition was performed with an alkali metal dispenser (SAES), and the amount of Cs was controlled by the evaporation current and time. In our experiments, the current was set to 5.7 A, and the time is less than 40 s. The work function was estimated to be slightly less than 2.5 eV after Cs deposition, since the photoemission at 1000 nm wavelength is still a two-photon mechanism (SI, Fig. S3). It is well known that less than 0.1ML Cs is required for such a strong reduction of the work function, see e.g., Ref[28].

Comment 2.8. There are several minor grammar mistakes throughout the manuscript (mostly superfluous "the"), and the manuscript would benefit from a close read.

Reply to 2.8: In the revised version, we have tried our best to fix the grammatical errors.

Reviewer #3 (Remarks to the Author):

The main finding reported in the manuscript is the observation of hyperbolic plasmon-polaritons (HPP) supported by two-dimensional crystals of MoOCl2 in the visible to the near-infrared range. Nevertheless, the previous publication "Visible-frequency hyperbolic plasmon polaritons in a natural van der Waals crystal", by Venturi, G., et al (Nat Commun 15, 9727, 2024), has recently shown and characterized the nanophotonics of HPP in MoOCl2. As a critical point, I could not find the citation of this reference in the manuscript. Moreover, the presented results do not add new aspects to the discussion provided in Venturi's work.
The use of PEEM to investigate the optical near field of bidimensional polaritonic media can be considered a novel technical approach, but the manuscript lacks presenting details on the technique and comparison to consolidated optical near field probes as s-SNOM. The work also lacks making quantitative comparison of the experimental results and data analysis with the simulations shown in the supplementary information. The results of polarization control and twisted crystals seem interesting but are only superficially discussed and no theoretical bases are provided to support and better describe the claimed control of the IFC and directionality. Therefore, I cannot recommend the publication. In the following, I list some points to be addressed to improve the work.

Reply: We thank the reviewer for his/her helpful comments. We have addressed all of the suggestions in the revised version. First, we have added a detailed description and discussion of the PEEM technique and comparison to s-SNOM in the revised Supporting Information, as shown in the response to ***Comment 3.2***.
Second, we have added the quantitative comparison of the experimental results with the simulated and theoretical results and added detailed discussions in the revised Supporting Information, mainly including the IFCs and dispersion relations, as shown in the reply to Reviewer #1's ***Comment 1.2* and *Comment 1.4***
Third, we have added some discussions on polarization control in the revised Supporting Information, as shown below.

Additional Changes in the manuscript in answer to this Comment: (see SI page 12):
The principle of polarization control is based on the fact that the hyperbolic plasmon mode is dominantly a TM-like mode, which can be verified from the intensity of each electric field component. As shown in Fig. S9, the intensity of $|E_x|$ is much larger than that of $|E_y|$, at a representative wavelength of 1000 nm, indicating the nature of TM-like mode. According to momentum conservation, at normal incidence, the in-plane wavevector compensation to excite the hyperbolic mode is completely provided by the Au nanoparticle. Under a given polarization, mainly the wavevectors excited from the Au nanoparticle along this polarization are coupled to the hyperbolic mode to compensate for the required wavevectors, which can be conveniently depicted in k space. It should be noted, the limitation of wavevectors provided by Au nanoparticle depends on its size, smaller size can excite higher wavevectors, but the coupling efficiency will be weaker for smaller nanoparticles due to the weaker scattering. For

polarization control, the main contribution in our work is the experimental realization of polarization control for hyperbolic modes at normal incidence, which has not been performed before.

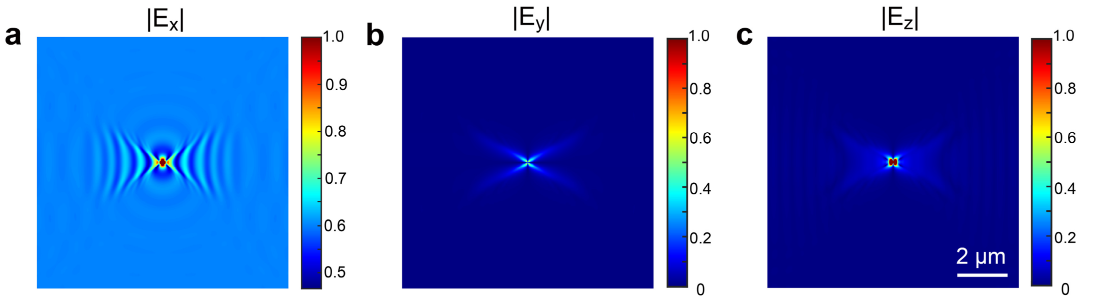

Fig. S9. Comparison of the intensity of each electric field component at the surface of $MoOCl_2$ (λ = 1000 nm).

Comment 3.1. Cite Venturi's work and point out the advances the manuscript presents.

Reply to 3.1: We have added related citations in the revised manuscripts as Ref. [22,23]. We appreciate Venturi's work and another related experimental work published very recently by Basov's group. We also appreciate the theoretical prediction of $MoOCl_2$ hyperbolic polaritons published several years ago (Ref. [16,17]), which directly inspired our PEEM experiments in the beginning. In our work, we measured the refractive index of $MoOCl_2$ by ourselves and detected the hyperbolic polaritons using PEEM. While hyperbolic modes have been extensively studied by s-SNOM, the shift to plasmons and near-IR frequencies allowed the observation by PEEM, which has not been used to image hyperbolic wavefronts before. And we are excited to perform the first PEEM experiment on hyperbolic polaritons.

We believe that both PEEM and SNOM have their own advantages. They are complementary methods for studying hyperbolic plasmons at near-infrared frequencies. In our PEEM experiments, we are able to perform fast direct imaging of hyperbolic modes at normal incidence, enabling high signal-to-noise ratio and straightforward imaging of hyperbolic modes, without the need for complicated data extraction (see also our reply to Reviewer #1's ***Comment 1.6***). In addition, PEEM is perfectly compatible with tunable femtosecond lasers, allowing convenient wavelength and polarization controls in our experiments (measured wavelength up to 1400 nm in this work). Such experimental conditions enable the acquisition of high-quality images, and further reconstruction of IFCs and dispersion relations.

Except for fundamental characterization of the hyperbolic modes supported by $MoOCl_2$, we also performed twist angle and polarization control, and the full IFCs of twist system were reconstructed for the first time as we know, benefited from the possibility of polarization control at normal incidence. In addition, we also demonstrated the possibility of constructing artificial structures on $MoOCl_2$ flake to manipulate its hyperbolic polaritons, which is essential for practical applications in the future.

Therefore, this study highlights PEEM as a highly effective method for nanoimaging polaritons in $MoOCl_2$. The polaritons were dynamically tailored and controlled through tunable light polarization, wavelength at normal incidence and interlayer twist, observed in both real and k spaces. Particularly, the full iso-frequency contours were reconstructed by incorporating polarization-selective excitations. In addition, we demonstrated the feasibility to manipulate polaritons using designed artificial structures on $MoOCl_2$. Thus, we believe that this work has sufficient new aspects for readers.

Changes in the manuscript in answer to Comment 3.1: Please see our changes in the manuscript in answer to Reviewer #1's **Comment 1.6**.

Comment 3.2. Improve the description of PEEM technique and provide details on how it can be used to probe the optical near field of polaritonic media. Provider for a comparison with s-SNOM.

Reply to 3.2: We have added a more detailed descriptions of the PEEM technique and probe details in the Supporting Information. In addition, we have also added some discussions of the comparison with s-SNOM in the Supporting Information. However, we would like to emphasize that we prefer to avoid any statement that PEEM is superior to s-SNOM. PEEM and s-SNOM are complementary methods for studying hyperbolic plasmons at near-infrared frequencies, each with its own advantages.

Changes in the manuscript in answer to Comment 3.2: In the Supporting Information, we have added a more detailed description of the PEEM technique and probe details (see SI page 18):

Photoemission electron microscopy (PEEM) is based on the photoelectric effect. Photoemission is a quantum electronic phenomenon in which electrons are emitted from the surface of a material by absorbing photon energies to overcome the work function. In PEEM, the photo-emitted electrons from the sample surface are collected by electron lenses to obtain an image (direct, non-scanning), resulting in spatial resolution down to 3 nm as reported[23]. In the field of near-field optics, the PEEM technique has been successfully applied to image the near-field modes, especially the plasmonic modes in metallic nanostructures.

The probe principle is very concise and relies on a multi-photon photoemission process to overcome the material's work function. That is, the nonlinear photoemission yield follows $P_E \propto I^N$, where P_E is the photoemission intensity, N is the nonlinear order (photon number), and I is the local light intensity; and $I \propto |\boldsymbol{E}|^2$, where $\boldsymbol{E}$ is the local electric field.

In addition, the probe depth is within a few nanometers of the surface in the visible and near-infrared ranges[24]. Thus, the PEEM image directly corresponds to the near-field intensity at the very sample surface. Note that in the near-infrared, the photoemission intensity can be enhanced by reducing the work function and thus the nonlinear order. A widely used method is to deposit a sub-monolayer of cesium (Cs) on the surface of the sample. With the help of Cs, the nonlinear order decreases to 2 in the near infrared, i.e., the nonlinear photoemission yield follows $P_E \propto I^2$ (the case in this work). This approach allows the near-field hyperbolic modes to be imaged on the surface of $MoOCl_2$.

In the Supporting Information, we have also added the discussion of comparison with s-SNOM (see SI page 19):

PEEM and s-SNOM are complementary methods for studying hyperbolic plasmons at near-infrared frequencies, each with its own advantages. In the last decade, mainly s-SNOM has been widely used to probe optical near-fields of hyperbolic materials with great universality. Working wavelengths range from the visible to the THz. In contrast, the upper wavelength range for PEEM is limited to the near infrared (generally UV-NIR) due to the requirement of overcoming the work function. The mode of operation of s-SNOM is tip scanning (photon in, photon out), while the mode of operation of PEEM is direct imaging (photon in, electron out). Sample requirements are relatively higher for PEEM compared to s-SNOM. A clean and conductive top surface is required to avoid surface charging and discharging during a PEEM measurement, while s-SNOM has no such constraints. In addition, electric and magnetic field control is possible in s-SNOM, while such control is more difficult in PEEM, although there are some reports on electric field control[25,26].

It is possible to obtain field intensity and phase information from the s-SNOM using a reference beam, while phase information is generally difficult (but not impossible) to obtain from PEEM.

Due to the non-scanning detection scheme, PEEM has the advantage of direct imaging. This leads to a faster detection scheme. The acquisition time of each image is typically 0.1-1.0 s, and multiple time averaging is often used only to further increase the signal-to-noise ratio. In addition, the field of view can be quickly switched (within a few seconds) from 100 μm to 0.75 μm with our PEEM type (ACSPELEEM III, Elmitec GmbH).

Furthermore, the non-scanning nature of PEEM results in very low near-field perturbation of the structured sample with high spatial resolution. PEEM is perfectly compatible with tunable femtosecond lasers in normal or oblique incidence, allowing convenient wavelength and polarization control and even time-resolved measurements on the fs time scale. For s-SNOM, oblique incidence from the front side is commonly used, but normal incidence has also been performed by transmission s-SNOM from the back side of the substrate[27].

We also include a table below comparing PEEM and s-SNOM. However, due to the rapid development of both techniques, we do not wish to include this table in the revised manuscript to avoid misinterpretation.

Table 1. Comparison of PEEM and s-SNOM.

Method	Working principle	Imaging manner	Wavelength range	Laser incidence	Sample requirement	Data processing	Best spatial resolution	Temperature	Electric/magnetic field control
s-SNOM	photon in, photon out	tip scanning, slow	visible-THz	commonly oblique	low	complex	<10 nm	low/room T	capable
PEEM	photon in, electron out	direct imaging, fast	UV-NIR	normal/oblique	high	simple	<10 nm	low/room T	hard

Comment 3.3. Improve data treatment. Extract polariton propagation profiles from the nanoparticles launchers, determine their momenta and construct the frequency-momentum dispersion relation that is a key property to understand the HPP's nanophotonics.

Reply to 3.3: The dispersion relation has already been presented in the Supporting Information (old Fig. S7). In the revised manuscript, we have further strengthened the comparisons with theoretical calculations using the transfer matrix method, which show close agreement. In particular, we have modified the old Fig. S7 and added corresponding descriptions.

Changes in the manuscript in answer to Comment 3.3: The revised contents in the Supporting Information are as follow (see SI pages 10-11):

We calculate the polariton dispersion relation by the transfer matrix method[21]. Our theoretical model is based on a three-layer structure: layer 1 ($z > 0$, air), layer 2 ($-d < z < 0$, $MoOCl_2$) and layer 3 ($z < -d$, glass), where z is the value of the vertical axis and d is the thickness of $MoOCl_2$ slab. We consider transverse magnetic modes and the corresponding Fresnel reflection coefficient r_p of this three-layer system is given by:

$$r_p = \frac{r_{12}+r_{23}e^{i2k_z^{(2)}d}}{1+r_{12}r_{23}e^{i2k_z^{(2)}d}} \quad (4)$$

$$r_{12} = \frac{Q_1-Q_2}{Q_1+Q_2} \quad (5)$$

$$r_{23} = \frac{Q_2-Q_3}{Q_2+Q_3} \quad (6)$$

$$Q_j = \frac{k_z^{(j)}}{\varepsilon_t^{(j)}} \quad (7)$$

$$k_z^{(j)} = \sqrt{\varepsilon_t^{(j)}\frac{\omega^2}{c^2} - \frac{\varepsilon_t^{(j)}}{\varepsilon_z^{(j)}}q^2} \quad (8)$$

$$\varepsilon_t^{(j)} = \varepsilon_x^{(j)}\cos^2\theta + \varepsilon_y^{(j)}\sin^2\theta \quad (9)$$

Here, $k_z^{(j)}$ is the out-of-plane wave vector, q is the in-plane wave vector, $\varepsilon_t^{(j)}$ is the tangential component of the in-plane dielectric function of layer j and θ is the angle relative to the x axis. r_{jk} represents the reflection coefficient of the interface between layer j and layer k. When $Im(r_p)$ reach peaks, the dispersion relation can be derived. It should be noted, the permittivity of $MoOCl_2$ used here is from our measurements. As shown in Fig S8c, the calculated and experimental dispersion relations are in good agreement. In addition, the calculated wavevector-thickness relation is also consistent with the experimental result (Fig S8f). These results indicate that our entire work is self-consistent.

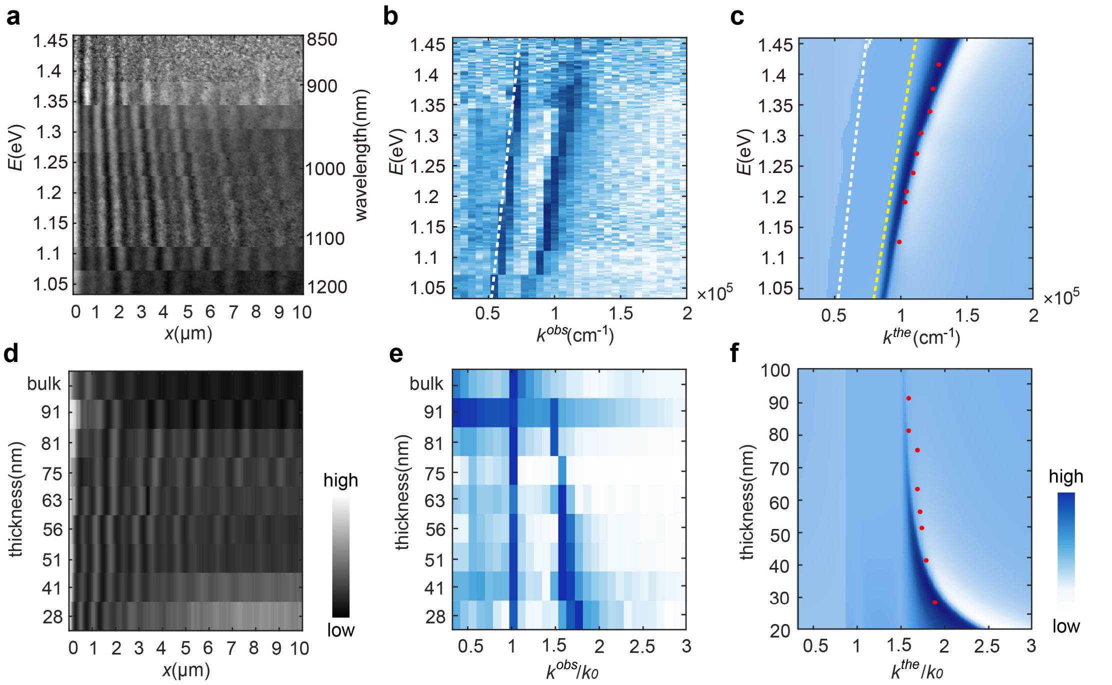

Fig. S8. Dispersion relation measured from $MoOCl_2$ sample edges and comparisons with theoretical calculations. (**a**) Wavelength-dependent near-field patterns on a straight sample edge (along the y-axis) of a ~60 nm $MoOCl_2$ flake excited with x-polarizations at normal incidence. (**b**) Extracted dispersion relation using FFT, in which the air mode and hyperbolic plasmon polariton mode can be observed. (**c**) Calculated polariton dispersion relation by transfer matrix method[21]. The red dots denote experimental results from (b). The white and yellow dashed lines denote air (k_0) and substrate ($1.5k_0$) modes. (**d,e**) Variations of near-field patterns and the corresponding FFT peaks with the thickness of $MoOCl_2$ (including bulk material), at a representative wavelength of 1000 nm. (**f**) Calculated polariton wavevector-thickness relation. The red dots denote experimental results from (e).

Comment 3.4. Explain the changes in the central part of the FFTs in Fig. 2b.

Reply to 3.4: In the revised manuscript, we have added many discussions on this issue, including comparisons of experimental data with theoretical calculations of hyperbolic and lenticular modes, as well as air and waveguide modes. Because the **Review#1** also pointed out similar issues in his/her ***Comments 1.2 and 1.4***, we have presented our explanations and revisions there, please check them for your convenience.

Comment 3.5. Verify why no HPP is seen for 700 nm excitation in Fig. 2 results. In Venturi's work HPPs are found around this wavelength.

Reply to 3.5: In fact, we can see HPP at 700 nm in Figure 2c, if we enlarge the image. However, we can only see 1−2 fringes, possibly due to the increased loss at short wavelengths and the poor signal-to-noise ratio compared to background signals. Even at 650 nm, we can still observe a faint fringe of HPP mode. This means that the HPP modes at 700 nm are difficult to observe in our PEEM experiments.

Changes in the manuscript in answer to Comment 3.5: We have added some descriptions in the main text (page 6): It should be noted that we can still observe 1−2 fringes of hyperbolic modes at 700 nm, but the visibility is very weak compared to that around 1000 nm.

Comment 3.6. Justify the use of 5 nm SiO2 @ 200 nm Au nanoparticles for polariton excitation, while larger metallic rod- or disk-like antennae, without dielectric coatings, are typically designed for such functionalities.

Reply to 3.6: We use Au nanoparticles because they can be conveniently obtained and transferred to the surface of $MoOCl_2$ flakes. Such a process is fast (within 2 min) and clean, causing as little damage as possible to $MoOCl_2$. Before performing experiments, we simulated the excitation effect of Au nanoparticles of different sizes and found that 200 nm was a well suitable choice.

For mid-infrared phonon polaritons, large metallic disks have generally been used. According to our understanding, as the polariton wavelength shifts to near-infrared, the size of the launcher should also decrease for better wavevector compensation. The wavevector compensation provided by the Au nanoparticles depends on their size, higher wavevectors can be excited with smaller Au nanoparticles. In fact, Au nanoparticles have been widely used to excite SPP on Au films, and the Au nanoparticle/Au film coupling structures have also been extensively investigated. We are very familiar with this research field of Au-based SPPs and LSPRs in the near infrared. Therefore, it's a natural choice to use Au nanoparticles as launchers. Of course, artificial metallic rod- and disk-like antennas can also be a suitable choice.

The 5 nm SiO_2 shell is a very useful trick for successful PEEM experiments. The main problem is the material-dependent intensity of the photoemission effect. The photoemission signals from bare Au nanoparticles are very strong due to the high free electron density of Au and the localized surface plasmon resonance (LSPR). Such strong photoemission will mask the signals from the $MoOCl_2$ surface, which has much weaker photoemission intensity. To reduce the photoemission intensity of Au nanoparticles, we coated them with 5 nm SiO_2 shells because the free-electron density of SiO_2 is much lower than that of Au.

Changes in the manuscript in answer to Comment 3.6: We have added some additional discussions in the Supporting Information (see SI pages 19-20):

We use Au nanoparticles because they can be conveniently obtained and transferred to the surface of $MoOCl_2$ flakes. Such a process is fast and clean, causing as little damage as possible to $MoOCl_2$.

Before performing experiments, we simulated the excitation effect of Au nanoparticles of different sizes and found that 200 nm was a well suitable choice. The simulated near-field modes with 5 nm SiO_2 @ 200 nm Au are shown in Fig. S5. The wavevector compensation provided by the Au nanoparticles depends on their size, higher wavevectors can be excited with smaller Au nanoparticles.

The 5 nm SiO_2 shell is a very useful trick for successful PEEM experiments. The main problem is the material-dependent intensity of the photoemission effect. The photoemission signals from bare Au nanoparticles are very strong due to the high free electron density of Au and the localized surface plasmon resonance (LSPR). Such strong photoemission will mask the signals from the $MoOCl_2$ surface, which has much weaker photoemission intensity.

To reduce the photoemission intensity of Au nanoparticles, we coated them with 5 nm SiO_2 shells because the free-electron density of SiO_2 is much lower than that of Au.

We have also added some additional discussions on the role of 5 nm SiO_2 shell in the Methods section of the revised main text (page 10): The 5 nm SiO_2 shell was used to reduce the photoemission intensity of bare Au nanoparticle, which is an essential trick for successful PEEM experiments.